Energy approach to consistent QED theory for calculation of electron-collision strengths: Ne-like ions

L. N. Ivanov,* E. P. Ivanova,* and L. V. Knight
296 ESC, Brigham Young University, Provo, Utah 84602
(Received 7 May 1993)

An energy approach based on consistent QED theory is outlined which presents the energy of any decaying atomic state in complex form with the imaginary part responsible for different types of decays. The aim is to study, in a uniform manner, elementary processes responsible for emission-line formation in plasmas. The energy approach is generalized here for the collisional problem. Numerical results on electron collisional strengths and rate coefficients for Ne-like ions are presented. It is shown that collisional rate coefficients are close to their maxima at an electron temperature $\sim 0.30 E_{\text{threshold}}$ for iron and $\sim 0.15 E_{\text{threshold}}$ for argon.

PACS number(s): 34.10.+x, 52.20.−j

I. INTRODUCTION

The x-ray laser problem has stimulated the development of theoretical methods for the modeling of multicharged ion emission lines in plasmas. The purpose of the present investigation is to study spectra line intensities in plasmas using a uniform advanced approach for the calculation of elementary process rate coefficients. The current trend is to study high-Z elements. The hope is to find lasing effects on the transitions of Ne-like or Ni-like ions. However, low-temperature plasma sources are more efficient and less expensive devices. They show promise for producing lasing in the vacuum ultraviolet (VUV) and soft x-ray region. Preliminary investigations of capillary spark discharge were made [1–4] which show the possibility of their use as plasma sources for the generation of a soft-x-ray or extreme ultraviolet amplified spontaneous emission (ASE). Recent experimental investigations [5–7] have shown that a capillary discharge is a highly efficient plasma source that promises to meet the conditions for lasing at definite transitions of multicharged ions. One approach is based on using a capillary discharge plasma which can be laser heated to temperatures of about 250 eV. This was shown by x-ray diagnostics [8,9]. In [8,9] it is shown that the plasma might be extremely uniform along the axis and that the electron density can be varied by changing the electrical energy supplied to the capillary.

Our atomic calculations [10,11] have identified several potential laser lines in a collisionally pumped neonlike or nickel-like plasma, and magnetohydrodynamic (MHD) modeling [12] has shown that a capillary discharge device should be capable of producing the appropriate plasma conditions to achieve a population inversion in some of these lines. An experiment is being constructed to evaluate the accuracy of the MHD model and investigate the possibility of observing an inversion in a neonlike argon or a nickel-like krypton plasma. It is necessary to search for the optimal plasma parameters to give efficient operation of capillary discharge device as a laser.

Two key problems must be solved in order to develop a code adequate to predict the plasma parameters needed to generate ASE: (1) accurate calculations of rate coefficients for elementary processes in the plasma that are responsible for the formation of emission lines; (2) kinetics calculations at definite plasma parameters to determine level populations, inversions, line intensities, and gain coefficients. The consideration of time evolution of emission lines together with the evolution of plasma parameters is of significant importance.

Under steady-state plasma conditions, two dominating elementary processes should be included: (a) electron-collisional excitation and deexcitation; (b) radiative relaxation of excited states. More sophisticated kinetics analysis demands the inclusion of the variety of other elementary processes, as well as the effects of their interference. We consider the inclusion of the high-lying Rydberg and autoionization Rydberg states of the ions of the previous ionization stage into kinetic scheme, to be one of the most important refinements of the "simplest" model.

The most elaborate codes for atomic calculations are based on different kinds of approximations to the multiconfiguration Dirac-Fock procedure developed in [13]. A brief review of these codes is given in [14], where the comparison of oscillator strengths of Ne-like ions resonance 2-3 transitions is given for six versions. The comparison shows that oscillator strengths differ sometimes by factors of 3–4. The disagreements in these very similar techniques are attributed to the different treatments of electron correlation. There is also no complete agreement between theories for 3-3 and 2-2 transitions [15,16]. These uncertainties in the ground spectroscopic data can in principle lead to a misleading picture of the plasma spectrum generated due to complicated multichannel atomic processes.

Another question of primary importance for the inves-

*Permanent address: Institute of Spectroscopy, Russian Academy of Sciences, Troitsk Moscow Region, 142092 Russia.

tigation of multichannel processes is the theoretical consistency for all stages of the calculation. Thus, a uniform, theoretically consistent approach to the whole problem is needed. Here, we try to develop such an approach for the calculation of the level populations in the simplified collisional-radiative model with a restricted number of reaction channels.

We present here the uniform energy approach (EA) formally based on the quantum electrodynamic (QED) theory, for the calculation of rate coefficients. The electron collision strengths and rate coefficients of excitation are calculated for Ne-like ions of argon, iron, and barium. To test the results of calculations we compare them with other authors' calculations and with available experimental data.

II. ENERGY APPROACH IN THE THEORY OF DECAYING ATOMIC STATES

Perturbation theory

The adiabatic Gell-Mann and Low GML formula for the state energy shift ΔE [17] with electrodynamic scattering matrix provides in principle a consistent QED approach in the theory of the stationary states. It yields for all excited states (that can decay due to either radiation or autoionization) a complex value [18]

$$\Delta E = \mathrm{Re}\Delta E + \mathrm{Im}\Delta E \tag{1}$$

with the decay probability $P = 2\,\mathrm{Im}\Delta E$. The latter can be presented as a sum of contributions of different physical channels with specific final states [19]. Of course, the final results for elementary processes coincide with those of the traditional amplitude approach. Nevertheless, we prefer the EA. It allows the application of the well-developed theory of degenerate and near-degenerate stationary states in the theory of the nonstationary states, thus accounting for elementary processes of a different physical nature as well as their interference in a uniform manner.

When studying complicated processes with many open reaction channels, one faces the problem of the consistency of approximations used at different stages of calculation. The widespread electric method (using the "best" available independently calculated values for different atomic characteristics) is doubtful, at least from a theoretical point of view. The EA automatically provides theoretical consistency. In the frame of EA one deals from the very beginning with the observable values—atomic line intensities and cross sections rather than with amplitudes. It simplifies the derivation of final expressions because amplitudes contain some redundant information of no physical sense.

To start with the QED GML formula, one must choose the zero-order approximation. Usually one uses for this purpose a one-electron Hamiltonian with a central potential that can be treated as a bare potential in the formally exact QED perturbation theory (PT). We are not concerned here with the QED-renormalization procedure as the related problems do not appear in the lowest orders of PT for the values under consideration. The bare potential includes the electric potential of the atomic nucleus and some model potential that is to be compensated for in all orders of PT. What are the main principles guiding the construction of the bare potential in the atomic theory?

The most widespread one is optimizing of the level positions, calculated in the first order of PT, possibly accounting for configuration interaction. The states of several configurations can be optimized simultaneously. This optimization principle is the essence of numerous versions of the self-consistent mean-field approximation and of the semiempirical fitting procedures, though the optimizing criteria can differ. A great number of level positions for different atoms and ions were predicted by these methods with high accuracy. The accuracy of the fitting procedures is typically higher than the accuracy of the physical model on which the procedure is formally based. But it is well known that optimizing the final state energies does not provide the reliability of the zero-order approximation, i.e., the quality of the individual electron energies and of the corresponding individual electron wave functions. Such functions do not represent the optimal basis for the consistent many-electron theory. It is manifested in the poor convergence of the PT expansion or in the poor convergence of the configurations superposition expansion. Of course this circumstance is of more principal importance for the other atomic characteristics than for level positions.

There are many well-known attempts to find the more fundamental optimization principles for the bare one-electron Hamiltonian or (what is the same) for the basis set of one-electron functions which represents such a Hamiltonian. One with the best theoretical foundation is known as the method of natural orbitals [20]. The diagonalizaiton of the "exact" one-electron density matrix of the many-electron system is accepted as the optimization principle in this method. Another simplified solution is known as the density-functional method. The minimization of th gauge noninvariant contribution of the lowest QED PT corrections is proposed in [21] as the "*ab initio*" optimization principle. In our calculations of different characteristics we dealt with atoms and ions having one, two, or three quasiparticles (electrons and vacancies) outside the core of closed shells. For example, the excited states $1s^2 2s^2 2p^5 nl$ of the Ne-like ion is a two-quasiparticle (2QP) state. We accept, as the bare potential, a potential including the electric nuclear potential and some parametrized potential that imitates the interaction of closed-shell electrons with quasiparticles. The parameters of the model bare potential are chosen so as to generate accurate eigenenergies of all one-quasiparticle (1QP) states, i.e., $1s2s^2 2p^6$, $1s^2 2s 2p^6$, $1s^2 2s^2 2p^5$ states of the F-like ion and $1s^2 2s^2 2p^6 nl$ states of Na-like ions, with the same nucleus. The individual quasiparticle eigenfunctions and eigenenergies satisfy the one-quasiparticle Dirac equation with model potential [22].

Further, this potential is used as a bare potential in the PT of states with any number of vacancies and electrons outside the same core. The way the input 1QP eigenenergies had been previously obtained (theoretically or experi-

mentally) does not mater. We assume that the "exact" 1QP energies are used to generate the zero-order approximation. To avoid accounting for the 1QP effects twice we omit the real parts of contributions of 1QP Feynman diagrams in orders of PT, thus the theoretical consistency is preserved. In contrast to the methods based on the optimization of the final theoretical energies our method provides the reliable level structure in the zero-order PT (at least for the two- and three-quasiparticle systems). It ensures better quality of the individual quasiparticle eigenfunctions and better convergence of the PT. The orbitals of quasiparticles are generally more compact in our calculations as compared with the previous ones and the cross sections are smaller, at least for the most intense transitions.

In the second order of the QED PT (or for the first order of the atomic PT) the energy shift is expressed in terms of two-electron matrix elements:

$$V(1,2;4,3)=\sqrt{(2j_1+1)(2j_2+1)(2j_3+1)(2j_4+1)}(-)^{j_1+j_2+j_3+j_4+m_1+m_2}\times\sum_{a,\mu}(1)^{\mu}\begin{bmatrix} j_1 & j_3 & a \\ m_1 & m_3 & \mu \end{bmatrix}\begin{bmatrix} j_2 & j_4 & a \\ m_2 & -m_4 & -\mu \end{bmatrix}Q_a(1,2;4,3)\ , \tag{2}$$

with

$$\begin{aligned}Q_a(1,2;4,3)=&R_a(1,2;4,3)S_a(1,2;4,3)+R_a(\tilde{1},2;4,\tilde{e})S_a(\tilde{1},2;4,\tilde{3})+R_a(1,\tilde{2};\tilde{4},3)S_a(1,\tilde{2};\tilde{4},3)+R_a(\tilde{1},\tilde{2};\tilde{4},\tilde{3})S_a(\tilde{1},\tilde{2};\tilde{4},\tilde{3})\\&+\sum_l R_l(1,2;\tilde{4},\tilde{3})S_a^l(1,2;\tilde{4},\tilde{3})+\sum_l R_l(\tilde{1},\tilde{2};4,3)S_a^l(\tilde{1},\tilde{2};4,3)\\&-\sum_l R_l(\tilde{1},2;\tilde{4},3)S_a^l(\tilde{1},2;\tilde{3},4)-\sum_l R_l(1,\tilde{2};4,\tilde{3})S_a^l(1,\tilde{2};4,\tilde{3})\ ,\end{aligned} \tag{3}$$

where $R_a(1,2;4,3)$ is the radial integral of the Coulomb interelectron interaction with large radial components; the tilde denotes a small component; the last four terms account for the magnetic interelectron interaction with l being space and a being total rank of interaction operator. For the Coulomb part the space and radial ranks coincide. The interelectron interaction in the lowest orders of QED PT is imitated by the photon propagator; its expansion over products of the tensor operators generates the a,μ expansion in (2).

In the QED theory of the excited states the Coulomb and magnetic radial integrals are complex values. The definition of all integrals and angular multiplyers S_a and S_a^l, with the detailed description of their calculation, have been given elsewhere [22,23].

It is worthwhile to emphasize that all electrons of the system (including the electrons of closed shells) are presented explicitly in the PT though the lowest orders include only eigenstates of quasiparticles. In our calculations the highest-order corrections are usually accounted for through the modification of the bare potential and the interaction of quasiparticles with each other, thus preserving the analytic form of the lowest-order corrections [24]. All the modifications approximate the contributions of th definite high-order Feynman diagrams (FD).

III. ENERGY APPROACH IN SCATTERING THEORY

When studying the electron-positron pair production in nuclear collisions [25] we generalized the EA to cover the problems of scattering theory. Here, we briefly outline the main idea using, as an example, the collisional deexcitation of the Ne-like ion: $((2j_{iv})^{-1}3j_{ie}[J_iM_i],\epsilon_{\rm in})\rightarrow(\Phi_0,\varepsilon_{\rm sc})$. Here, Φ_0 is the state of the ion with closed shells (ground sate of the Ne-like ion), J_i is the total angular moment of the initial target state, indices iv, ie are related to the initial states of vacancy and electron, indices and $\varepsilon_{\rm in}$ and $\varepsilon_{\rm sc}$ are the incident and scattered energies, respectively to the incident and scattered electrons, respectively. In the second-quantization representation, the initial state of the system "atom plus free electron" can be written as

$$|I\rangle=a_{\rm in}^{\dagger}\sum_{m_{ie},m_{iv}}a_{ie}^{\dagger}a_{iv}\Phi_0\tilde{C}^{J_iM_i}_{m_{ie},m_{iv}}\ , \tag{4}$$

with

$$\tilde{C}^{J_iM-i}_{m_{ie},m_{iv}}=\sqrt{2J_i+1}(-1)^{j_{ie}-m_{ie}}\begin{bmatrix} j_{ie} & j_{iv} & J_i \\ m_{ie} & -m_{iv} & -M_i \end{bmatrix} \tag{5}$$

being Clebsh-Gordan coefficient with the additional phase multiplier accounting for tensor properties of the annihilation operator a_{iv}. Final state is

$$|F\rangle=a_{\rm sc}^{\dagger}\Phi_0\ , \tag{6}$$

where Φ_0 is the state of an ion with closed electron shells (ground state of Ne-like ion), $|I\rangle$ represents three-quasiparticle (3QP) state, and $|F\rangle$ represents the 1QP state. Quantum numbers of the free-electron states are not specified yet.

To justify the EA in the scattering problem, we suppose that the system "atom plus electron" was placed at the time $t\rightarrow-\infty$ in a potential box of large but finite size. All the states (4) and (6) of a confined system are stationary, their eigenenergies are quantized. The box

effect at $t \to -\infty$ can be described by the additional potential V_b; its concrete form is of no matter. Next, we use traditional procedures which provide automatically the $\mathrm{Im}\Delta E$ for the states that become nonstationary during adiabatic evolution of the potential, namely, we (i) introduce the time-dependent box potential $V_b[1-\exp(\alpha t)]$, $\alpha > 0$, thus at any time $t < 0$ we deal only with the stationary states, however, the box potential disappears as $t \to 0$; (ii) treat $-V_b \exp(\alpha t)$ as a perturbation on an equal footing with the interaction of quasiparticles with each other; (iii) calculate the energy shifts δE of all states (4) at $t < 0$ using the GML formula for the stationary states; (iv) assume $t = 0$, $\alpha = 0$ in the final expression.

For the state (4) the scattering part of $\mathrm{Im}\Delta E$ appears first in the second order of atomic PT in the form of the integral over the scattered electron energy ε_{sc}:

$$\int d\varepsilon_{sc} G(\varepsilon_{iv}, \varepsilon_{ie}, \varepsilon_{in}, \varepsilon_{sc}) / (\varepsilon_{sc} - \varepsilon_{iv} - \varepsilon_{ie} - \varepsilon_{in} - i0) , \quad (7)$$

with

$$\mathrm{Im}\Delta E = \pi G(\varepsilon_{iv}, \varepsilon_{ie}, \varepsilon_{in}, \varepsilon_{sc}) . \quad (8)$$

Here, G is a definite squared combination of the two-electron matrix elements (3). The value

$$\sigma = -2\,\mathrm{Im}\Delta E \quad (9)$$

represents the collisional cross section if the incident electron eigenfunction is normalized by the unit flow condition, and the scattered electron eigenfunction is normalized by the energy δ function.

The next step, mixing of the near-degenerated atomic states, accounts for the highest-order corrections of a specific type. To obtain the complex eigenenergies in the frame of the rigorous theory of the near-degenerate stationary states [26] one must diagonalize the complex secular matrix $\langle I'|M|I\rangle$ calculated between the states (4). In the lowest order, the secular matrix coincides with the usual energy matrix. It should be emphasized that in the lowest order of the consistent PT one must take the same ε_{in} for all the states to be mixed and zero-order scattering energy $\varepsilon_{sc} = \varepsilon_{iv} + \varepsilon_{ie} - \varepsilon_{in}$. Refinement of ε_{sc} using the "more accurate" transition energies effectively accounts for the highest-order corrections. At least part of these corrections will be accounted for the second time while mixing the near-degenerated states. Accounting for the same effects twice is a common shortcoming of the eclectic calculations.

The simplified diagonalization procedure is widely used in practice. Usually one diagonalizes only the real part of the secular matrix, yielding a real matrix of eigenvectors coefficients B^{IK}_{iv,ie,J_i}. The matrix realizes the transition from the pure-jj-coupling representation to the representation where eigenstates are numerated by numbers I,K. The diagonal elements of the transformed matrix

$$\langle IK'|M|IK\rangle = \sum_{iv',ie'} \sum_{iv,ie} B^{IK'}_{iv',ie'} \langle iv',ie',J_i|M|iv,ie,J_i\rangle B^{IK}_{iv,ie,J_i} \quad (10)$$

represent the cross sections of the collisional deexcitation $(|IK,\varepsilon_{in}j_{in}) \to (\Phi_0,\varepsilon_{sc}j_{sc})$. The uncertainties in cross sections arising from this approximation are of the order $\mathrm{Im}\Delta E/\delta E$, where δE is the typical distance between the mixing states of the target [19].

The elements of the secular matrix are representable by the energy FD. Each diagram describes the concrete virtual process and can be classified in accordance with the number of the real target quasiparticles involved in this process. In the first and the second orders of atomic PT, there exist only vacuum, 1QP, 2QP, and 3QP diagrams. The energy shift of any system (with any number of quasiparticles outside the same core), can be expressed in terms of the contributions of these diagrams. Vacuum diagrams have no end lines. 1QP, 2QP, and 3QP diagrams have one, two, and three pairs of end lines, correspondingly. Generally, vacuum diagrams are not considered as they contribute only the energy of the closed shells common for all states, i.e., they do not manifest themselves in any observable process. The real part of 1QP diagrams in all orders must be omitted, too, according to the special choice of zero approximation. The $\mathrm{Im}\langle|M|\rangle$ related to the collisional transitions appears first in the second PT order; it is represented by the 2QP and 3QP diagrams. These diagrams are considered in Secs. IV and V. As mentioned above, the highest-order corrections are accounted for effectively through modification of the bare potential and the potential of interquasiparticle interaction.

IV. COLLISIONAL TRANSITIONS WITH PARTICIPATION OF THE GROUND STATE: DEEXCITATION AND EXCITATION

The deexcitation process is presented in the second order by the only 3QP diagram (the so-called annihilation diagram) since the transition to the final state without quasiparticles can be formally considered as quasiparticle annihilation. The diagram is shown in Fig. 1. Let us discuss briefly the diagram's elements. The end and the

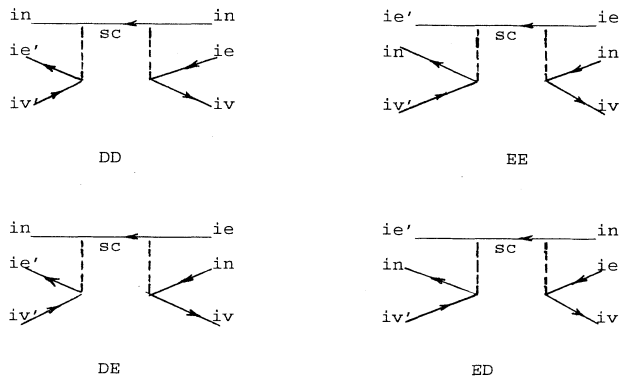

FIG. 1. 3QP annihilation diagram, describing the deexcitation of the 2QP target. Direct-direct, exchange-exchange, direct-exchange, and exchange-direct versions are shown. Each version accounts for the direct (D) or exchange (E) interaction of the incident electron with the "bra" or "ket" target states.

inner solid lines directed from the right to the left are labeled by the electron state indices. Those directed from the left to the right are labeled by the indices of the vacancy states. The end lines indicated by the indices (ie',iv') are related to the "bra" state in $\langle I',|M|I\rangle$. Those indicated by the indices (ie,iv) to the "ket" state. Bra lines are assumed to be continued infinitely to the left; ket lines are assumed to be continued infinitely to the right. All possible versions of indexing of the end lines are shown on the Fig. 1. The central section of each diagram has an imaginary line drawn between two vertices (two dashed lines of the diagram). It generally intersects several inner and end quasiparticle lines. Their indices must be attributed to the final state of the system "atom plus free electron." In the case under consideration there is only one such line with index sc. It means that the final state is one-quasiparticle state with one free electron outside the target with closed shells.

Rather complicated combinations of $3jm$ symbols appear in the angular parts of matrix elements, especially in the case of the "excited-excited" transitions. The summation over all m numbers is greatly simplified due to use of the momentum diagram techniques [27,28]. The starting momentum diagram consists of the core part that is topologically equivalent to the corresponding FD and two additional bar and ket fragments that link all the bra-quasiparticle lines and all the ket-quasiparticle lines. The topology of these fragments reflect the scheme of individual quasiparticle angular moment coupling [29]. The summation over all m numbers is reduced to a transformation of momentum diagram according to simple rules [30]. An example of such a transformation is given in Sec. V.

Here, we only note that the partial cross section for the transition between states (4) and (6) depends on $j_{\rm in},j_{\rm sc},m_{\rm in},m_{\rm sc},M_i$. The numerical summation over $j_{\rm in},j_{\rm sc}$ is assumed. The dependence on magnetic quantum numbers is eliminated in the amplitude approach by introducing the total angular moment J_T of the system "atom plus free electron" with subsequent summation over J_T [30]. This elimination occurs in the energy diagrams automatically, without introducing J_T. This simplification is especially significant in the case of "excited-excited" transitions.

The collisional strength $\Omega(I\to F)$ is widely used instead of the cross section $\sigma(I\to F)$. These values are connected with one another as follows:

$$\sigma(I\to F)=\Omega(I\to F)\frac{\pi}{(2J_i+1)\varepsilon_{\rm in}[(\alpha Z)^2\varepsilon_{\rm in}+2]} \tag{11}$$

(relativistic formula). Here and below the Coulomb units are used: 1 C.u.$\approx 27.054Z^2$ eV, for energy; 1 C.u.$\approx 0.529\times 10^{-8}/Z$ cm for length 1 C.u.$\approx 2.419\times 10^{-17}/Z^2$ sec for time. Z is the nucleus charge and α is the fine structure constant. To simplify the comparison with the formulas of the amplitude approach we rearranged the final expression for the deexcitation cross section so as to pick out the amplitudelike combination:

$$\sigma(IK\to 0)=2\pi\sum_{j_{\rm in},j_{\rm sc}}(2j_{\rm sc}+1)\left[\sum_{j_{ie},j_{iv}}\langle 0|j_{\rm in},j_{\rm sc}|j_{ie},j_{iv},J_i\rangle B^{IK}_{ie,iv}\right]^2, \tag{12}$$

where the amplitudelike combination

$$\langle 0|j_{\rm in},j_{\rm sc}|j_{ie},j_{iv},J_i\rangle=\sqrt{(2j_{ie}+1)(2j_{iv}+1)}(-1)^{j_{ie}+1/2}$$
$$\times\sum_{\lambda}(-1)^{\lambda+J_i}\left[\delta_{\lambda,J_i}\frac{1}{2J_i+1}Q_\lambda({\rm sc},ie;iv,{\rm in})+\begin{Bmatrix} j_{\rm in} & j_{\rm sc} & J_i\\ j_{ie} & j_{iv} & \lambda\end{Bmatrix}Q_\lambda(ie,{\rm in};iv,{\rm sc})\right]. \tag{13}$$

Upon substituting the two-term expression (13) into (12), one gets four terms corresponding to the four diagram versions in Fig. 1: direct-direct, direct-exchange, exchange-direct, and exchange-exchange. The version name reflects the type of interaction (direct or exchange) of the free electron with the target in the bra and ket states.

For the collisional excitations from the ground state (inverse process), we consider $a^\dagger_{\rm in}\Phi_0$ as the initial state, and

$$|F\rangle=a^\dagger_{\rm sc}\sum_{m_{fe},m_{fv}}a^\dagger_{fe}a_{fv}\Phi_0\tilde{C}^{J_fM_f}_{m_{fe},m_{fv}} \tag{14}$$

as a final state. The cross section is

$$\sigma(0\to IF)=2\pi(2J_f+1)\sum_{j_{\rm in},j_{\rm sc}}(2j_{\rm sc}+1)\left[\sum_{j_{fe},j_{fv}}B^{FK}_{fe,fv}\langle j_{fe},j_{fv}J_f|j_{\rm in},j_{\rm sc}|0\rangle\right]^2, \tag{15}$$

with

$$\langle j_{fe},j_{fv},J_f|j_{\rm in},j_{\rm sc}|0\rangle=\sqrt{(2j_{fe}+1)(2j_{fv}+1)}(-1)^{j_{fe}+1/2}$$
$$\times\sum_{\lambda}(-1)^{\lambda+J_f}\left[\delta_{\lambda,J_f}\frac{1}{2J_f+1}Q_\lambda({\rm sc},ie;iv,{\rm in})+\begin{Bmatrix} j_{\rm in} & j_{\rm sc} & J_f\\ j_{fv} & j_{fe} & \lambda\end{Bmatrix}Q_\lambda(fe,{\rm sc};fv,{\rm in})\right]. \tag{16}$$

It is worthwhile to remember, that the different normalization conditions are used for the incident and for the scattered electron wave functions. Upon accounting for the normalization multipliers (see Appendix) one gets symmetrical expressions for the excitation and deexcitation, saving the weight multiplier $2J_f+1$ in (15).

V. EXCITED-EXCITED COLLISIONAL TRANSITIONS

The state (4) is accepted as the initial and the state (14)—as the final in the "excited-excited" transition. Three energy digrams describe this process. Four versions of each diagram are shown in Fig. 2. The first eight 2QP digrams describe pure electron or pure vacancy transitions, resulting from the immediate interaction of the free electron with an excited electron or vacancy. The free line denotes the spectator (or passive) quasiparticle which does not participate in the process directly. The last four 3QP diagrams describe the processes that change the states of both quasiparticles of the target, the bound electron, and the vacancy. The section of each diagram, drawn between two vertices, intersects three lines (one of them is the inner line with index sc), i.e., here we deal with the 3QP final state. Let us emphasize that the total moments J_f of the final states are not specified yet. The diagrams represent the summary cross section of the transitions to all final states with the particular electron configuration of the target rather than to concrete states. The quantum numbers of the concrete final states are introduced below as the result of the diagram transformation.

The momentum diagram technique is illustrated by the direct electron-exchange vacancy diagram (D_vE_e). The starting momentum diagram is shown in Fig. 3. The bra and ket fragments are on the left and on the right sides of two dotted lines. According to general rules, every line of momentum diagram carries two indices, j and m: the rank of the definite tensor operator and the index of its particular component. Summation over all m is assumed. Summation over index M_i of the line J_i realizes averaging over the magnetic quantum numbers of the initial state. Two elementary reduction rules, graphically shown in Figs. 4(a) and 4(b), simplify the diagram if the latter includes the corresponding "elementary" fragments, triangles, and loops. Otherwise the "preliminary" transformation, shown in Fig. 4(c), can be used to preform the "elementary" fragments. Each preliminary transformation implements additional summation over the auxiliary moment I. Using these simple rules, one can reduce step by step any diagram to the single line carrying the δ function. The diagram contribution will be expressed in terms of $6j$ Racah symbols with summation over all auxiliary moments. Any moment diagram of the second order is reducible to the single line due to a two-step "preliminary" transformation and a sequence of the "elemen-

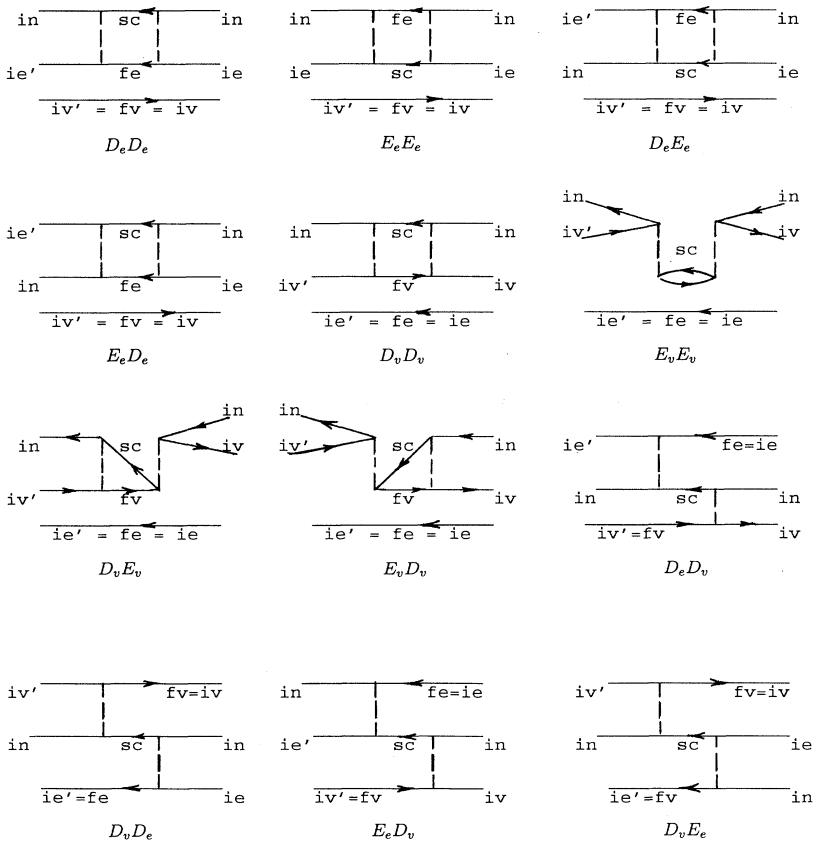

FIG. 2. The diagrams, describing collisional transition between excited 2QP of the target. The first eight 2QP diagrams describe transitions with changing of only one quasiparticle state of the target. The last four 3QP diagrams describe the transitions with changing of both quasiparticle states of the target. Capital letters indicate direct or exchange interaction of the target with the incident electron in the "bra" or in the "ket" state. Small letters indicate with quasiparticle (electron or vacancy) changes its state.

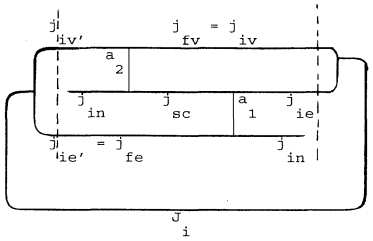

FIG. 3. Momentum diagram corresponding to the $D_v E_e$ FD. The dotted lines cut off the "bra" and "ket" fragments.

tary" transformations. The resulting expressions have the form of the double summation $\sum_{I_1,I_2}$ over auxiliary moments I_1, I_2. There are several alternative variants to choose the "preliminary" transformations, leading to alternative equivalent forms of the final expression. For each starting moment digram, corresponding to the FD of Fig. 2, one of the "preliminary" transformations had been chosen to link the final states lines fe and fv. The corresponding auxiliary moment can be identified with the final-state total moment J_f. This allows the representation of the total cross-section as a sum over concrete reaction channels in the jj-coupling scheme. Both steps of the "preliminary" transformation of the diagram $D_v E_e$ are shown in Fig. 5. The same two-step transformation

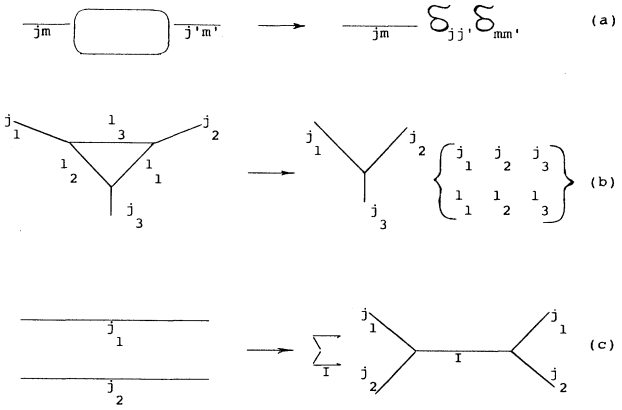

FIG. 4. Two "elementary" (a),(b) and "preliminary" (c) transformations. The set of these transformations reduces any momentum diagram to the single line.

followed by the set of obvious "elementary" transformations reduces any of the second-order diagrams to the single line.

Similar to previous case, we rearranged the final expression for the cross section to pick out the amplitudelike combination. In the intermediate-coupling-scheme representation, the cross section of the collisional excited-excited $IK \rightarrow IF$ transition looks as follows:

$$\sigma(IK\rightarrow FK)=\frac{\pi}{2}\sum_{j_{\rm in},j_{\rm sc}}(2j_{\rm sc}+1)\sum_{I}(2I+1)\left[\sum_{j_{ie},j_{iv}}\sum_{j_{fe},j_{fv}}(2J_F+1)[B^{FK}_{fe,fv}\langle j_{ef},j_{vf},J_f|I,j_{\rm in},j_{\rm sc}|j_{ie},j_{iv},J_i\rangle B^{IK}_{ie,ve}]\right]^2, \tag{17}$$

with the amplitudelike combination depending on the auxiliary moment I. In the amplitude approach, every amplitude depends on its own auxiliary moment. Thus the cross-section expression in that approach include two independent auxiliary summations [30].

The amplitudelike combination consists of the electron and vacancy parts:

$$\langle\,|\,|\rangle=\langle\,|\,|\rangle_{\rm el}+\langle\,|\,|\rangle_{\rm vac}\ . \tag{18}$$

Substituting the two-term expression (18) into (17), one gets four combinations that can be related to the purely electron, to the purely vacancy, and electron-vacancy diagrams of Fig. 2. The electron and vacancy parts of the amplitudelike combinations can be represented in turn as a sum of the direct and exchange parts.

The electron contribution is

$$\langle\,|I,j_{\rm in},j_{\rm sc}|\,\rangle_{\rm el}=\delta_{iv,fv}\sqrt{(2j_{ie}+1)(2j_{iv}+1)(2j_{fe}+1)(2j_{fv}+1)}\begin{Bmatrix} I & J_f & J_i \\ j_{iv} & j_{ie} & j_{fe}\end{Bmatrix}$$
$$\times\sum_{a,I}(-1)^{a+1/2+j_{iv}+j_{ie}+j_{fe}}\left[\delta_{a,I}\frac{1}{2I+1}Q_a(\mathrm{sc},fe;ie,\mathrm{in})+\begin{Bmatrix} I & j_{\rm sc} & j_{\rm in} \\ a & j_{fe} & j_{ie}\end{Bmatrix}Q_a(\mathrm{sc},fe;\mathrm{in},ie)\right]. \tag{19}$$

In the direct part, auxiliary moment I coincides with the total rank of the interaction a.

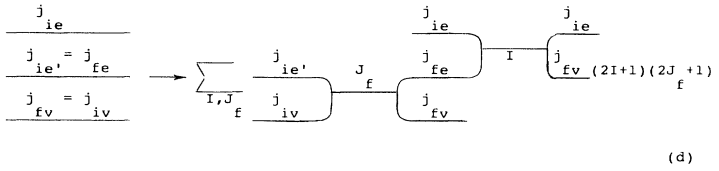

FIG. 5. Two-step "preliminary" transformation. Each momentum diagram of this work can be reduced to the single due to this "preliminary" transformation and a set of "elementary" transformations.

The vacancy contribution is

$$\langle |I, j_{\rm in}, j_{\rm sc}| \rangle_{\rm vac} = \delta_{ie,fe} \sqrt{(2j_{ie}+1)(2j_{iv}+1)(2j_{fe}+1)(2j_{fv}+1)} \begin{Bmatrix} I & J_f & J_i \\ j_{ie} & j_{iv} & j_{fv} \end{Bmatrix}$$
$$\times \sum_{a,I} (-1)^{1/2+j_{ie}+J_i+J_f} \left[\delta_{a,I} \frac{1}{2I+1} Q_a({\rm sc}, iv; fv, {\rm in}) + \begin{Bmatrix} I & j_{\rm sc} & j_{\rm in} \\ a & j_{iv} & j_{ie} \end{Bmatrix} Q_a({\rm sc}, iv; {\rm in}, fv) \right] . \quad (20)$$

VI. NUMERICAL RESULTS

The above theory is applied here to investigate electron-collisional cross sections and rate coefficients for Ne-like ions excitations. Radiative recombination rates for these ions have been investigated in [15, 23] using the same theory. Rates for both elementary processes will be used then in the kinetics calculations for Ne-like ion pop-

TABLE I. Energy levels of Ne-like ions Ar IX and Fe XVII (units are cm^{-1}).

	Ar IX ($Z=18$)				Fe XVII ($Z=26$)				
No.	Level	J	Expt. [34]	Theory Present work	Level	J	Expt. [35]	Theory Present work	Theory [31]
1	$2s\ \ 2p$	0	0	0	$2s\ \ 2p$	0	0	0	0
2	$2p_{3/2}\ 3s_{1/2}$	2	2 026 542	2 026 504	$2p_{3/2}\ 3s_{1/2}$	2	5 849 320	5 849 054	5 855 681
3	$2p_{3/2}\ 3s_{1/2}$	1	2 033 120	2 033 273	$2p_{3/2}\ 3s_{1/2}$	1	5 864 590	5 864 708	5 871 662
4	$2p_{1/2}\ 3s_{1/2}$	0	2 044 670	2 044 390	$2p_{1/2}\ 3s_{1/2}$	0	5 951 212	5 950 805	5 956 518
5	$2p_{1/2}\ 3s_{1/2}$	1	2 051 880	2 052 270	$2p_{1/2}\ 3s_{1/2}$	1	5 960 870	5 960 998	5 967 008
6	$2p_{3/2}\ 3p_{3/2}$	1	2 149 320	2 149 800	$2p_{3/2}\ 3p_{1/2}$	1	6 093 407	6 093 153	6 099 089
7	$2p_{3/2}\ 3p_{3/2}$	3	2 169 894	2 169 600	$2p_{3/2}\ 3p_{1/2}$	2	6 121 606	6 121 033	6 128 677
8	$2p_{3/2}\ 3p_{1/2}$	2	2 170 923	2 170 620	$2p_{3/2}\ 3p_{3/2}$	3	6 134 630	6 134 044	6 141 047
9	$2p_{3/2}\ 3p_{1/2}$	1	2 176 716	2 176 320	$2p_{3/2}\ 3p_{3/2}$	1	6 143 730	6 142 989	6 150 493
10	$2p_{3/2}\ 3p_{3/2}$	2	2 182 224	2 181 790	$2p_{3/2}\ 3p_{3/2}$	2	6 158 360	6 157 278	6 164 853
11	$2p_{1/2}\ 3p_{1/2}$	1	2 189 330	2 188 900	$2p_{3/2}\ 3p_{3/2}$	0	6 202 450	6 201 869	6 211 008
12	$2p_{1/2}\ 3p_{1/2}$	0	2 192 240	2 191 620	$2p_{1/2}\ 3p_{1/2}$	1	6 219 114	6 219 605	6 225 625
13	$2p_{1/2}\ 3p_{3/2}$	2	2 195 230	2 194 790	$2p_{1/2}\ 3p_{3/2}$	1	6 245 225	6 244 090	6 250 816
14	$2p_{1/2}\ 3p_{3/2}$	1	2 196 230	2 195 540	$2p_{1/2}\ 3p_{3/2}$	2	6 248 350	6 247 741	6 254 324
15	$2p_{3/2}\ 3p_{3/2}$	0	2 265 320	2 275 360	$2p_{1/2}\ 3p_{1/2}$	0	6 353 230	6 363 845	6 382 883
16	$2p_{3/2}\ 3d_{3/2}$	0	2 349 300	2 348 603	$2p_{3/2}\ 3d_{3/2}$	0	6 463 942	6 462 790	6 471 451
17	$2p_{3/2}\ 3d_{3/2}$	1	2 351 420	2 350 700	$2p_{3/2}\ 3d_{3/2}$	1	6 472 500	6 470 917	6 479 930
18	$2p_{3/2}\ 3d_{5/2}$	2	2 355 570	2 354 950	$2p_{3/2}\ 3d_{5/2}$	2	6 486 288	6 485 900	6 495 791
19	$2p_{3/2}\ 3d_{5/2}$	4	2 358 730	2 358 660	$2p_{3/2}\ 3d_{5/2}$	4	6 486 530	6 487 059	6 497 860
20	$2p_{3/2}\ 3d_{3/2}$	3	2 361 760	2 361 960	$2p_{3/2}\ 3d_{3/2}$	3	6 492 788	6 493 559	6 502 404
21	$2p_{3/2}\ 3d_{3/2}$	2	2 366 960	2 366 990	$2p_{3/2}\ 3d_{3/2}$	2	6 506 650	6 506 800	6 516 087
22	$2p_{3/2}\ 3d_{5/2}$	3	2 370 655	2 371 530	$2p_{3/2}\ 3d_{5/2}$	3	6 515 320	6 515 800	6 526 494
23	$2p_{3/2}\ 3d_{5/2}$	1	2 381 120	2 381 490	$2p_{3/2}\ 3d_{5/2}$	1	6 552 200	6 547 857	6 564 054
24	$2p_{1/2}\ 3d_{3/2}$	2	2 382 450	2 382 700	$2p_{1/2}\ 3d_{3/2}$	2	6 594 461	6 594 789	6 602 675
25	$2p_{1/2}\ 3d_{5/2}$	3	2 384 880	2 385 380	$2p_{1/2}\ 3d_{5/2}$	2	6 606 500	6 600 953	6 610 544
26	$2p_{1/2}\ 3d_{5/2}$	2	2 385 380	2 385 430	$2p_{1/2}\ 3d_{5/2}$	3	6 606 500	6 605 908	6 615 598
27	$2p_{1/2}\ 3d_{3/2}$	1	2 411 310	2 418 700	$2p_{1/2}\ 3d_{3/2}$	1	6 660 000	6 666 952	6 679 234
28	$2s_{1/2}\ 3s_{1/2}$	1		2 639 720	$2s_{1/2}\ 3s_{1/2}$	1		6 932 114	6 951 738
29	$2s_{1/2}\ 3s_{1/2}$	0		2 668 780	$2s_{1/2}\ 3s_{1/2}$	0		6 986 582	7 005 493
30	$2s_{1/2}\ 3p_{1/2}$	0		2 780 200	$2s_{1/2}\ 3p_{1/2}$	0		7 196 098	7 216 068
31	$2s_{1/2}\ 3p_{1/2}$	1		2 781 050	$2s_{1/2}\ 3p_{1/2}$	1		7 199 894	7 219 978
32	$2s_{1/2}\ 3p_{3/2}$	2		2 783 390	$2s_{1/2}\ 3p_{3/2}$	2		7 218 806	7 238 595
33	$2s_{1/2}\ 3p_{3/2}$	1	2 791 700	2 792 670	$2s_{1/2}\ 3p_{3/2}$	1		7 233 790	7 254 052
34	$2s_{1/2}\ 3d_{3/2}$	1		2 967 370	$2s_{1/2}\ 3d_{3/2}$	1		7 560 137	7 580 521
35	$2s_{1/2}\ 3d_{3/2}$	2		2 967 470	$2s_{1/2}\ 3d_{3/2}$	2		7 561 509	7 582 528
36	$2s_{1/2}\ 3d_{5/2}$	3		2 967 600	$2s_{1/2}\ 3d_{5/2}$	3		7 563 671	7 585 978
37	$2s_{1/2}\ 3d_{5/2}$	2		2 984 800	$2s_{1/2}\ 3d_{5/2}$	2		7 606 710	7 625 118

ulations in a plasma. The numerical investigation is accomplished here for argon and iron in the Ne-like state. Level populations and line intensities of Ne-like argon are needed for the search for the optimal conditions in the plasma of a capillary discharge for lasing generation in a collisionally radiative scheme. Presently spectroscopic characteristics of multicharged iron states are under thorough theoretical and experimental investigation because of the broad need for these data for many applications. To test our theory we compare our calculations on collisional cross sections for Ne-like iron with known calculations [31,32]. Another test is conducted here by comparison with experimental data of Ref. [33], where few collision transitions in Ne-like barium were studied.

In Table I our calculations of energy levels for Ne-like argon and iron are given. A description of our method for energy-level calculation is presented in [24]. The first-order PT correction is calculated exactly, the high-order contributions are taken into account effectively: "polarization" interaction of two above-core quasiparti-

TABLE II. Electron-collision strengths for excitations from the ground state of Ne-like iron (incident electron energy $E=76.83$ Ry). Two approximations are given: (a) first order of the PT; (b) first order of the PT+effective accounting for the high PT orders corrections. Results are compared with the theory [31]. Our cross section of excitation (in cm^2) calculated with the accounting for high PT orders are in the last column. The numbers in brackets denote multiplicative powers of ten.

	Electron collision strengths			Excitation
	Present theory			cross section
Transition	(a)	(b)	Theory Ref. [31]	(present work)
1-2	1.144[−03]	1.073[−03]	1.351[−03]	1.227[−21]
3	1.214[−03]	2.603[−03]	2.439[−03]	2.978[−21]
4	2.252[−04]	2.118[−04]	2.730[−04]	2.423[−22]
5	1.086[−03]	2.227[−03]	2.266[−03]	2.547[−21]
6	3.327[−03]	2.772[−03]	3.550[−03]	3.171[−21]
7	2.730[−03]	3.032[−03]	3.581[−03]	3.468[−21]
8	3.411[−03]	2.966[−03]	3.889[−03]	3.393[−21]
9	1.236[−03]	1.033[−03]	1.375[−03]	1.181[−21]
10	2.196[−03]	2.572[−03]	3.178[−03]	2.942[−21]
11	2.740[−03]	2.683[−03]	3.142[−03]	3.069[−21]
12	1.338[−03]	1.144[−03]	1.466[−03]	1.308[−21]
13	1.410[−03]	1.154[−03]	1.560[−03]	1.320[−21]
14	2.615[−03]	3.057[−03]	3.826[−03]	3.497[−21]
15	4.938[−02]	4.009[−02]	4.567[−02]	4.586[−20]
16	1.380[−03]	1.417[−03]	1.661[−03]	1.620[−21]
17	4.247[−03]	4.464[−03]	5.030[−03]	5.106[−21]
18	5.306[−03]	5.530[−03]	6.499[−03]	6.326[−21]
19	4.827[−03]	4.744[−03]	5.693[−03]	5.426[−21]
20	3.536[−03]	3.692[−03]	4.317[−03]	4.221[−21]
21	1.889[−03]	1.865[−03]	2.313[−03]	2.133[−21]
22	2.466[−03]	2.694[−03]	3.165[−03]	3.081[−21]
23	2.428[−02]	2.778[−02]	2.517[−02]	3.177[−20]
24	2.256[−03]	2.201[−03]	2.682[−03]	2.518[−21]
25	2.976[−03]	2.930[−03]	3.517[−03]	3.350[−21]
26	2.989[−03]	3.207[−03]	3.834[−03]	3.669[−21]
27	7.094[−02]	1.042[−01]	1.058[−01]	1.192[−19]
28	9.674[−04]	8.179[−04]	9.570[−04]	9.355[−22]
29	1.861[−02]	1.596[−02]	1.590[−02]	1.825[−20]
30	2.013[−04]	2.059[−04]	2.500[−04]	2.348[−22]
31	6.427[−04]	8.833[−04]	9.190[−04]	1.010[−21]
32	1.006[−03]	1.019[−03]	1.278[−03]	1.165[−21]
33	7.982[−04]	2.514[−03]	2.070[−03]	2.876[−21]
34	1.520[−03]	1.519[−03]	1.773[−03]	1.738[−21]
35	2.570[−03]	2.574[−03]	3.004[−03]	2.945[−21]
36	3.576[−03]	3.570[−03]	4.139[−03]	4.083[−21]
37	1.016[−02]	1.398[−02]	1.438[−02]	1.600[−20]

TABLE III. Comparison of measured [33] and calculated electron-collisional excitation cross sections (σ) for Ne-like barium for two values of incident electron energy. (Units are 10^{-21} cm^2.)

		Measured [33]		Theory			
				Present work		[36]	[37]
Level	J	Level energy (eV)	$4\pi\frac{d\sigma}{d\Omega}(90°)$	Level energy (eV)	σ	σ	σ
			$E(el)=5.69$ keV				
Sum ($J=0$)			2.50±0.35		2.48	2.58	2.60
$2p_{3/2}\ 3d_{5/2}$	1	4937	3.98±0.56	4937.7	3.20	3.44	3.56
$2p_{1/2}\ 3d_{3/2}$	1	5295	2.12±0.30	5295.9	1.78	2.42	2.00
			$E(el)=8.20$ keV				
Sum ($J=0$)			2.27±0.32		1.83	1.89	1.94
$2p_{3/2}\ 3d_{5/2}$	1		3.30±0.46		2.87	2.99	3.23
$2p_{1/2}\ 3d_{3/2}$	1		1.82±0.25		1.64	2.10	1.82

cles and the effect of their "mutual screening." It should be noted that strong compensation of different PT terms is a characteristic feature of the states with vacancies in the core. This is one of the main reasons for the fact that the accuracy of conventional *a priori* calculations of such states does not always satisfy the requirements arising in some applications. This compensation becomes stronger with increasing nuclear charge. It manifests the crucial role of the theoretical self-consistency of the approach to the whole problem.

A comparison with experimental energy levels [34,35] shows that the typical discrepancy between our theoretical and experimental values is several hundreds of cm^{-1}. Two states are the exceptions: No. 15 ($J=0$) in $2p^5 3p$ and No. 27 in $2p^5 3d$. For these terms the calculational uncertainty is several thousand cm^{-1} and is practically

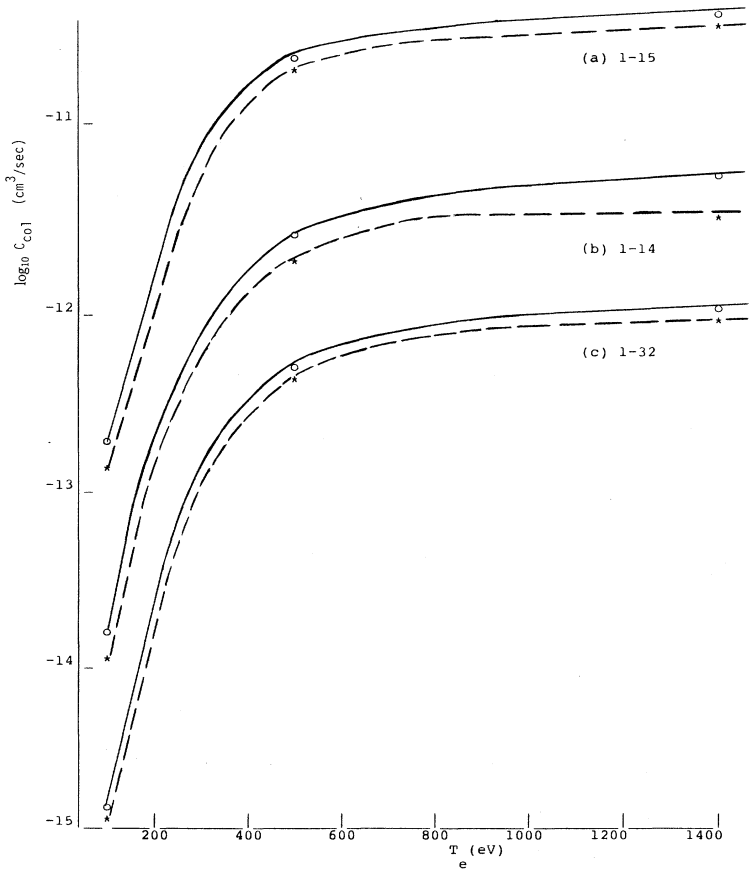

FIG. 6. Temperature dependence of some rate coefficients for electron-collisional excitations of Ne-like iron. The solid line corresponds to the calculation [32]; the dashed line corresponds to the present calculation (a) transition 1-15; (b) transition 1-14; (c) transiton 1-32 (see Table I for designation of levels).

independent of Z. Comparison with experimental energies encourage us to believe in the accuracy for highly excited states for which there is no experimental information.

Our results on electron collision strengths and cross sections of excitation from the ground state for Ne-like iron are given in Table II. Summation over j_{in}, j_{sc} in (16) spreads over the range $1/2-23/2$. We investigated numerically the convergency of this sum. It turned out that the highest partial-wave contribution is less than 1% for all states considered. The incident electron energy $E_{el}=76.83$ Ry $=$ 1045.4 eV was chosen for comparison with the corresponding data of Ref. [31]. Our results are presented in two approximations: (a) accounting for only first-order PT contributions in the secular matrix; (b) with the effective inclusion of the high-order corrections mentioned above. For some levels these corrections change the results by a factor of 2–3. As it was expected, our final collisional strengths appeared to be smaller (typically by 10–30 %) than those of Refs. [31,32].

In both cases (argon and iron) the collisional strengths have been calculated for the three reference values of the incident electron energy and then approximated by a simple analytical formula with "exact" asymptotics. The latter have been used in the convolution relativistic formula for the rate coefficients. The comparison of our collisional rate coefficients for iron with those from [32] is shown in Fig. 6. Their dependence on the electron temperature is shown for three different transitions. Like the cross sections, our rate coefficients are typically less than

TABLE IV. Electron-collision strengths for the Ne-like argon excitations from the ground state. E is impact electron energy. The numbers in brackets denote multiplicative powers of ten.

Transition \ E (eV)	425	500	750
1-2	2.377[−03]	2.036[−03]	1.303[−03]
3	6.583[−03]	7.566[−03]	9.017[−03]
4	4.736[−04]	4.048[−04]	2.587[−04]
5	1.468[−02]	1.761[−02]	2.241[−02]
6	6.300[−03]	5.437[−03]	3.456[−03]
7	7.219[−03]	5.012[−03]	2.911[−03]
8	6.238[−03]	5.824[−03]	4.795[−03]
9	2.173[−03]	1.794[−03]	1.033[−03]
10	6.770[−03]	6.794[−03]	6.451[−03]
11	2.029[−03]	1.675[−03]	9.641[−04]
12	1.604[−03]	1.079[−03]	8.794[−04]
13	8.090[−03]	8.140[−03]	7.814[−03]
14	1.793[−03]	1.488[−03]	8.561[−04]
15	8.607[−02]	8.758[−02]	8.670[−02]
16	2.807[−03]	2.197[−03]	1.136[−03]
17	8.829[−03]	7.091[−03]	4.129[−03]
18	1.296[−02]	1.041[−02]	5.227[−03]
19	9.348[−03]	7.180[−03]	3.512[−03]
20	7.349[−03]	6.082[−03]	3.994[−03]
21	4.374[−03]	3.325[−03]	1.579[−03]
22	6.110[−03]	5.854[−03]	5.623[−03]
23	1.463[−02]	1.552[−02]	1.866[−02]
24	3.658[−03]	2.744[−03]	1.254[−02]
25	6.086[−03]	5.532[−03]	4.763[−03]
26	3.919[−03]	2.939[−03]	1.341[−03]
27	2.632[−01]	2.933[−01]	3.725[−01]
28	1.926[−03]	1.561[−03]	8.504[−04]
29	3.128[−02]	3.219[−02]	8.670[−02]
30	4.332[−04]	3.544[−04]	2.129[−04]
31	1.383[−03]	1.201[−03]	8.918[−04]
32	2.152[−03]	1.764[−03]	1.066[−03]
33	5.089[−03]	7.505[−03]	1.323[−02]
34	3.082[−03]	2.428[−03]	1.264[−03]
35	5.155[−03]	4.060[−03]	2.116[−03]
36	7.220[−03]	5.681[−03]	2.956[−03]
37	2.387[−02]	2.818[−02]	3.771[−02]

those of Ref. [32]. It should be noted that inclusion into consideration of Rydberg and autoionization Rydberg states of ions of the previous ionization stage will definitely increase collisional rates. The method which allows treatment of these states on an equal basis with the adjacent continua has been elaborated in the scattering theory [25]. The numerical calculations on this subject are in the progress. The experimental information about the electron-collisional cross sections for high charged Ne-like ions is very scarce, and is extracted from indirect observations. Such experimental information for a few collisional excitations of the Ne-like barium ground state had been obtained in [33]. (Two electron-collisional energies were used in [33].) Table III compares these experimental results with our calculations and with those of two other theoretical works [36,37]. No obvious discrepancies between theoretical and experimental values for the considered states are found. Our results are at the lower margin of experimental error with one exception: for the state $2p_{3/2}3d_{5/2}$ $[J=1]$ our cross section at collisional energy 5.69 keV is a few percent lower. It should be noted that extraction of the cross section from the experiment is the most ambiguous for this level.

Our results for cross sections of excitation of Ne-like argon from the ground state are presented in Table IV. The corresponding results for rate coefficients are given in Table V. As far as we know there is only scarce information on electron-collision excitations of Ne-like argon.

TABLE V. Rate coefficients for electron-collision excitation of Ne-like argon at six values of electron temperatures T_e.

Transition \ T_e (eV)	Rate coefficients (cm^3/sec) 30	45	60	90	120	150
1-2	9.79[−14]	1.28[−12]	4.38[−12]	1.38[−11]	2.30[−11]	2.99[−11]
3	9.52[−14]	1.46[−12]	5.68[−12]	2.19[−11]	4.25[−11]	6.27[−11]
4	1.82[−14]	2.44[−13]	8.43[−12]	2.69[−12]	4.50[−12]	5.88[−12]
5	1.55[−13]	2.58[−12]	1.06[−11]	4.36[−11]	8.83[−11]	1.34[−10]
6	1.48[−13]	2.29[−12]	8.56[−12]	2.95[−11]	5.14[−11]	6.87[−11]
7	2.60[−13]	3.95[−12]	1.43[−11]	4.66[−11]	7.74[−11]	9.98[−11]
8	1.19[−13]	1.92[−12]	7.36[−12]	2.63[−11]	4.73[−11]	6.50[−11]
9	5.03[−14]	8.01[−13]	3.01[−12]	1.04[−11]	1.80[−11]	2.40[−11]
10	1.03[−13]	1.73[−12]	6.81[−12]	2.54[−11]	4.72[−11]	6.67[−11]
11	4.45[−14]	7.20[−13]	2.73[−12]	9.51[−12]	1.66[−11]	2.21[−11]
12	5.95[−14]	9.21[−13]	3.36[−12]	1.10[−11]	1.83[−11]	2.36[−11]
13	1.17[−13]	2.00[−12]	7.94[−12]	2.99[−11]	5.58[−11]	7.91[−11]
14	3.75[−14]	6.14[−13]	2.35[−12]	8.22[−12]	1.44[−11]	1.92[−11]
15	9.07[−13]	1.72[−11]	7.23[−11]	2.88[−10]	5.52[−10]	7.96[−10]
16	3.33[−14]	6.64[−13]	2.79[−12]	1.06[−11]	1.93[−11]	2.63[−11]
17	1.01[−13]	2.03[−12]	8.55[−12]	3.29[−11]	6.01[−11]	8.25[−11]
18	1.49[−13]	3.00[−12]	1.27[−11]	4.86[−11]	8.83[−11]	1.21[−10]
19	1.09[−13]	2.19[−12]	9.23[−12]	3.53[−11]	6.41[−11]	8.73[−11]
20	7.78[−14]	1.59[−12]	6.77[−12]	2.64[−11]	4.88[−11]	6.77[−11]
21	4.97[−14]	1.01[−12]	4.28[−12]	1.64[−11]	2.98[−11]	4.06[−11]
22	5.14[−14]	1.09[−12]	4.78[−12]	1.97[−11]	3.80[−11]	5.48[−11]
23	1.04[−13]	2.27[−12]	1.02[−11]	4.39[−11]	8.83[−11]	1.32[−10]
24	3.93[−14]	8.16[−13]	3.49[−12]	1.35[−11]	2.45[−11]	3.34[−11]
25	5.21[−14]	1.11[−12]	4.89[−12]	1.99[−11]	3.80[−11]	5.43[−11]
26	4.16[−14]	8.67[−13]	3.71[−12]	1.44[−11]	2.62[−11]	3.57[−11]
27	1.44[−14]	3.38[−11]	1.59[−10]	7.19[−10]	1.50[−09]	2.29[−09]
28	5.89[−15]	1.76[−13]	9.09[−13]	4.28[−12]	8.66[−12]	1.26[−11]
29	1.08[−13]	3.26[−12]	1.71[−11]	8.63[−11]	1.95[−10]	3.24[−10]
30	7.10[−16]	2.58[−14]	1.47[−13]	7.62[−13]	1.62[−12]	2.45[−12]
31	2.18[−15]	8.01[−14]	4.59[−13]	2.43[−12]	5.28[−12]	8.10[−12]
32	3.47[−15]	1.27[−13]	7.22[−13]	3.77[−12]	8.04[−12]	1.21[−11]
33	4.70[−15]	2.05[−13]	1.37[−12]	9.17[−12]	2.39[−11]	4.27[−11]
34	2.22[−15]	1.04[−13]	6.68[−13]	3.91[−12]	8.81[−12]	1.37[−11]
35	3.72[−15]	1.74[−13]	1.12[−12]	6.54[−12]	1.47[−11]	2.29[−11]
36	5.21[−15]	2.43[−13]	1.56[−12]	9.16[−12]	2.06[−11]	3.21[−11]
37	1.37[−14]	7.12[−13]	4.99[−12]	3.39[−11]	8.63[−11]	1.49[−10]

For example, one can find theoretical and experimental intensities for several lines of Ne-like argon and chlorine in θ-pinch plasma at electron temperature ~ 65 eV and electron density $\sim 2.5\times 10^{16}$ cm^{-3} [38].

At this stage of our calculations the conclusion can be drawn that remarkable population of $2p^5 3p$ levels can be obtained at electron temperatures of 250–300 eV for iron and 40–50 eV for argon. Note that at 40–50 eV the abundance of Ne-like argon in a plasma is significant. Thus we believe that the results of the present theoretical investigation encourage once more the search for efficient laser schemes using $3p$-$3s$ transitions of Ne-like argon.

The comprehensive theoretical analysis of plasma spectra at different values of electron density and temperature also needs the special consideration of additional reaction channels. The results of such work will be presented in a future paper where the level populations and line intensities will be analyzed with their dependence on plasma parameters.

APPENDIX: NORMALIZATION OF FREE-ELECTRON WAVE FUNCTIONS

When calculating corrections of the PT to the energy of a stationary state one deals with the matrix elements that depend on the individual quasiparticles states and virtual bound and free-electron states. All the bound-state functions must be normalized to unity; all the free-electron-state functions to energy δ function. The same is true for the cross-section calculation. However, the incident-electron-state function must asymptotically coincide with the plane wave normalied to unit flow. We expand this wave over spherical partial waves, each of which satisfies the one-electron Dirac equation. The norm of each partial wave is unambiguously defined by the above asymptotic condition.

Radial components "f" (large) and "g" (small) of the individual electron state satisfy the radial Dirac equations

$$f' = -f(\kappa+|\kappa|)/r - gX_2 \ , \qquad g' = g(\kappa-|\kappa|)/r + fX_1 \ , \tag{A1}$$

$$X_1 = (\varepsilon - U)Z\alpha \ , \qquad X_2 = (\varepsilon + 2(Z\alpha)^{-2} - U)Z\alpha \ . \tag{A2}$$

Here, κ is the angular Dirac quantum number, U is the bare potential, and ε is the eigenenergy (positive for the free-electron state). The main r dependence of f and g at $r\to 0$ has been factored out [22], so that as $r\to 0$, $f\to$const, $g\sim r$ for $\kappa<0$, and $f\sim r$, $g\to$const for $\kappa>0$. To obtain the properly normalized cross section one must (i) perform all the calculations with the arbitrary normalized $f_{\rm in}$, $g_{\rm in}$, and $f_{\rm sc}$, $g_{\rm sc}$; (ii) multiply all the partial cross sections by the normalization multipliers $N^2_{\rm in}$, $N^2_{\rm sc}$ with

$$N^2_{\rm in} = Z\alpha\pi(2j_{\rm in}+1)\lim_{r\to\infty}\frac{1}{\sqrt{X_1X_2}\,Y(f_{\rm in},g_{\rm in})} \ , \tag{A3}$$

$$N^2_{\rm sc} = \frac{Z\alpha}{\pi}\lim_{r\to\infty}\frac{\sqrt{X_1X_2}}{Y(f_{\rm sc},g_{\rm sc})} \ , \tag{A4}$$

$$Y(f,g) = r^{2|\kappa|}(X_1f^2 + X_2g^2) \ . \tag{A5}$$

Two terms in (A5) are asymptoticallly proportional to $\sin(\omega r)^2$, and $\cos(\omega r)^2$, that provides convergence of the above expressions.

ACKNOWLEDGMENT

The authors would like to thank B. Peterson for his careful reading of the manuscript and for his many helpful comments.

[1] P. Bogen, H. Conrads, and R. Rusbuldt, Z. Phys. **186**, 240 (1965).
[2] R. A. McCorcle, Appl. Phys. A **26**, 261 (1981).
[3] J. J. Rocca, D. C. Beethe, and M. C. Marconi, Opt. Lett. **13**, 565 (1988).
[4] B. G. Peterson, K. J. Gray, G. W. Hart, and L. V. Knight, Bull. Am. Phys. Soc. **34**, 2095 (1989).
[5] C. Steden and H.-J. Kunze, Phys. Lett. A **151**, 1534 (1990).
[6] J. J. Rocca, M. C. Marconi, B. T. Szapiro, and J. Meyer, Proc. SPIE **1551**, 275 (1991).
[7] J. J. Rocca, O. D. Cortazar, B. Szapiro, K. Floyd, and F. G. Tomasel, Phys. Rev. E **47**, 1299 (1993).
[8] A. Zigler, M. Kishenevsky, M. Givon, E. Yarkoni, and B. Arad, Phys. Rev. A **35**, 4446 (1987).
[9] N. Edison, P. E. Young, N. Holmes, R. W. Lee, N. C. Woolsey, J. S. Wark, and W. J. Blyth, Phys. Rev. E **47**, 1305 (1993).
[10] L. V. Knight, A. M. Panin, B. G. Peterson, and E. P. Ivanova, in Proceedings of the International Conference *Laser 92* (STS, McLean, VA, 1993), p. 113.
[11] E. P. Ivanova and A. V. Gulov (unpublished).
[12] J. Lin, M.S. thesis, Brigham Young University (1992) (unpublished).
[13] I. P. Grant, B. J. McKenzie, P. H. Norrington, D. F. Mayers, and N. C. Pyper, Comput. Phys. Commun. **21**, 207 (1980).
[14] D. H. Sampson, H. L. Zhang, A. K. Mohanty, and R. E. H. Clark, Phys. Rev. A **40**, 604 (1989).
[15] E. P. Ivanova and A. V. Gulov, Phys. Lett. A **140**, 39 (1989).
[16] R. R. Haar, L. J. Curtis, N. Reinstad, C. Jupen, and I. Martinson, Phys. Scr. **35**, 296 (1987).
[17] M. Gell-Mann and F. Low, Phys. Rev. **84**, 350 (1951).
[18] Yu. Yu. Dmitriev, G. L. Klimchitskaya, and L. N. Labzovskii, *Relativistic Effects in Spectra of Atomic Systems* (Energoatomizdat, Moscow, 1984).
[19] M. N. Driker and I. N. Ivanov, Sov. J. Opt. Spectrosc. **49**, 209 (1980).
[20] E. R. Davidson, Rev. Mod. Phys. **44**, 451 (1972); E. R. Davidson and D. Feller, J. Chem. Phys. **74**, 3977 (1981).
[21] A. V. Glushkov and L. N. Ivanov, Phys. Lett. **70A**, 33 (1992).

[22] L. N. Ivanov, E. P. Ivanova, and E. V. Aglitskii, Phys. Rep. **164**, 315 (1988).
[23] E. P. Ivanova and A. V. Gulov, At. Data Nucl. Data Tables **49**, 1 (1991).
[24] E. P. Ivanova, L. N. Ivanov, A. V. Glushkov, and A. E. Kramida, Phys. Scr. **32**, 513 (1985).
[25] L. N. Ivanov and T. V. Zueva, Phys. Scr. **43**, 368 374 (1991).
[26] V. V. Tolmachev, Adv. Chem. Phys. **14**, 421, 471 (1969).
[27] A. P. Yutsis, I. B. Levinson, and V. V. Vanagas, *Mathematical Apparatus for Angular Momentum Theory* (Mintis, Vilnius, 1960) (in Russian).
[28] B. R. Judd, *Second Quantization in Atomic Spectroscopy* (Johns Hopkins, Baltimore, MD, 1967).
[29] L. N. Ivanov and V. V. Tolmachev, Sov. Phys. J. **12**, 199 (1969).
[30] A. Bar-Shalom, M. Klapish, and J. Oreg, Phys. Rev. A **38**, 1773 (1988).
[31] A. K. Bhatia and G. A. Doschek, At. Data Nucl. Data Tables **52**, 2 (1982).
[32] P. L. Hagelstein and R. K. Jung, At. Data Nucl. Data Tables **37**, 121 (1987).
[33] R. E. Marrs, M. A. Levine, D. A. Knapp, and J. R. Henderson, Phys. Rev. Lett. **60**, 1715 (1988).
[34] A. E. Kramida, Kandidate thesis, Lebedev's Institute of Physics of Russian Academy of Sciences, Moscow (1983) (unpublished).
[35] C. Jupen and U. Litzen, Phys. Scr. **30**, 112 (1984).
[36] H. Zhang, D. H. Sampson, R. E. H. Clark, and J. B. Mann, At. Data Nucl. Data Tables **37**, 17 (1987).
[37] K. J. Reed, Phys. Rev. A **37**, 1791 (1988).
[38] R. C. Elton, R. U. Datla, J. R. Roberts, and A. K. Bhatia, Phys. Rev. A **40**, 4142 (1989).